4. M. Suarez and G. B. Schuster, *J. Am. Chem. Soc.* **117**, 6732 (1995).
5. S. Zahn and J. W. Canary, *Angew. Chem. Int. Ed. Engl.* **37**, 305 (1998).
6. L. Zelikovich, J. Libman, A. Shanzer, *Nature* **374**, 790 (1995).
7. V. Goulle, A. Harriman, J. M. Lehn, *J. Chem. Soc. Chem. Commun.* **1993**, 1034 (1993).
8. S. Shinkai, K. Inuzuka, O. Miyazaki, O. Manbe, *J. Am. Chem. Soc.* **107**, 3950 (1985).
9. G. De Santis, L. Fabbrizzi, M. Licchelli, P. Pallavicini, A. Perotti, *J. Chem. Soc. Dalton Trans.* **1992**, 3283 (1992).
10. N. Armaroli *et al.*, *J. Am. Chem. Soc.* **121**, 4397 (1999).
11. S. Muñoz and G. W. Gokel, *J. Am. Chem. Soc.* **115**, 4899 (1993).
12. P. R. Ashton *et al.*, *J. Am. Chem. Soc.* **121**, 3951 (1999).
13. C. Westermeier, H.-C. Gollmeier, J. Daub, *J. Chem. Soc. Chem. Commun.* **1999**, 2427 (1999).
14. M. Porsch, G. Siglseifert, J. Daub, *Adv. Mater.* **9**, 635 (1997).
15. D.-K. Yang, X.-Y. Huang, Y.-M. Zhu, *Annu. Rev. Mater. Sci.* **27**, 117 (1997).
16. C. Mao, W. Sun, Z. Shen, N. C. Seeman, *Nature* **397**, 144 (1999).
17. R. A. Bissell, E. Córdova, A. E. Kaifer, J. F. Stoddart, *Nature* **369**, 133 (1994).
18. J. W. Canary, C. S. Allen, J. M. Castagnetto, Y. Wang, *J. Am. Chem. Soc.* **117**, 8484 (1995).
19. J. W. Canary *et al.*, *Enantiomer*, in press.
20. S. Zahn and J. W. Canary, *Org. Lett.* **1**, 861 (1999).
21. J. W. Canary *et al.*, *Inorg. Chem.* **37**, 6255 (1998).
22. J. M. Castagnetto, X. Xu, N. Berova, J. W. Canary, *Chirality* **9**, 616 (1997).
23. K. Nakanishi and N. Berova, in *Circular Dichroism: Principles and Applications*, K. Nakanishi, N. Berova, R. W. Woody, Eds. (VCH, New York, 1994), pp. 361–398.
24. Z. Tyeklár and K. D. Karlin, in *Bioinorganic Chemistry of Copper*, A. Tyeklár and K. D. Karlin, Eds. (Chapman & Hall, New York, 1993), pp. 277–291.
25. Ligands **1** and **2** were synthesized by the alkylation of L-methionine or its methyl ester with two equivalents of 2-bromomethylquinoline in the presence of $NaHCO_3$ in dimethylformamide. Ligand **5** was prepared from stilbene-4-carboxaldehyde, which was reacted with the mono-triphenylphosphonium salt of 2,6-dibromomethylpyridine to yield 6-bromomethyl-2-vinyl-stilbenyl pyridine. The alkylation of methionine was carried out similar to that of **2**. All new compounds were characterized by standard spectroscopic means and gave satisfactory elemental analysis.
26. In a typical experiment, 0.35 ml of a 0.3 mM solution of **3** was placed in a 1-mm pathlength cell. After recording the CD spectrum, 0.011 ml of a 10 mM solution of ascorbic acid was added to the solution, and another CD spectrum was recorded. Adding 0.011 ml of a 10 mM solution of ammonium persulfate and recording the CD spectrum completed one cycle.
27. A. E. Siegrist, H. R. Meyer, P. Gassman, S. Moss, *Helv. Chim. Acta* **63**, 1311 (1980).
28. SPARTAN 5.1, Wavefunction, Inc., Irvine, CA.
29. We thank H. Barcena and J. McBride for help with electrochemical measurements. This work was supported by NIH grant GM49170.

30 November 1999; accepted 5 April 2000

Quantifying Denitrification and Its Effect on Ozone Recovery

A. Tabazadeh,[1]* M. L. Santee,[2] M. Y. Danilin,[3] H. C. Pumphrey,[4] P. A. Newman,[5] P. J. Hamill,[6] J. L. Mergenthaler[7]

Upper Atmosphere Research Satellite observations indicate that extensive denitrification without significant dehydration currently occurs only in the Antarctic during mid to late June. The fact that denitrification occurs in a relatively warm month in the Antarctic raises concern about the likelihood of its occurrence and associated effects on ozone recovery in a colder and possibly more humid future Arctic lower stratosphere. Polar stratospheric cloud lifetimes required for Arctic denitrification to occur in the future are presented and contrasted against the current Antarctic cloud lifetimes. Model calculations show that widespread severe denitrification could enhance future Arctic ozone loss by up to 30%.

Polar stratospheric clouds (PSCs) play important roles in the formation of the springtime Antarctic "ozone hole" by activating chlorine and denitrifying the stratosphere (*1*–*7*). Although similar abundances of reactive chlorine have been measured in both polar vortices (*8*–*12*), ozone loss has typically been much less severe over the Arctic than over the Antarctic (*1*, *2*). The Arctic vortex has generally been warmer, weaker, less persistent, and more distorted than the Antarctic vortex (*13*, *14*), and consequently up to now the Arctic has been less susceptible to ozone depletion. Although there has been significant ozone loss in the Arctic, especially in the coldest winters of the last decade (*1*, *2*, *15*–*19*), the magnitude of such loss has been partially masked by transport of ozone-rich air from higher altitudes (*16*–*21*). It has been suggested (*6*, *7*) that the observed lack of widespread severe denitrification in the Arctic (*22*–*24*) may be a major factor currently preventing the formation of an Arctic "ozone hole."

Here, the concept of "PSC lifetime" is introduced to explore how long a PSC must persist in the winter for denitrification to occur, and why the event currently occurs in the Antarctic but not in the Arctic. "PSC lifetime" is defined as the average time an air mass is exposed to temperatures below the condensation point of thermodynamically known solid PSC particle phases, such as nitric acid trihydrate (NAT), nitric acid dihydrate (NAD), and ice.

Some studies have implied that Arctic denitrification has contributed to ozone depletion inside the Arctic vortex during the coldest winters of the last decade (*15*, *25*). Others (*26*–*31*) suggest that simultaneous loss of ozone and reactive nitrogen in the Arctic is often a result of dynamical mixing of different air masses and is unrelated to denitrification. Also, most in situ and balloon data sets (*25*, *32*–*36*) showing denitrification in the Arctic were collected near mountainous terrain, where lee waves could have strongly affected the local reactive nitrogen (*37*) [or water vapor (*38*)] profile through small-scale cloud processing. Overall, the fact that satellite data (*22*–*24*) show no indication of widespread denitrification in the Arctic at present may suggest that the local perturbations caused by lee waves are not of global or regional significance, in terms of leading to a substantial irreversible removal of nitric acid vapor. However, lee wave–generated PSCs may still play a role in Arctic ozone depletion by providing additional surface areas upon which chlorine activation can occur (*39*).

Here we examine both denitrification and dehydration of the Antarctic polar vortex in 1992 by correlating the depletion in nitric acid (*40*) and water vapor (*41*) concentrations, measured by Microwave Limb Sounder (MLS), with the increase in aerosol extinction (*42*) measured by Cryogenic Limb Array Etalon Spectrometer (CLAES). To identify the onset and duration of denitrification and dehydration in the Antarctic, we generated daily maps of gas phase nitric acid, water vapor, and aerosol extinction for different potential temperature surfaces from early May through November. Figure 1 shows daily polar maps for selected dates during the Antarctic winter of 1992 interpolated onto the 450 K potential temperature surface. A denitrified or dehydrated region is defined as an area in which nitric acid or water vapor mixing ratios, as seen by MLS, are depleted below 2 parts per billion by volume (ppbv) and 3 parts per million by volume (ppmv), respectively, without a significant corresponding increase in aerosol extinction, indicating the absence of solid nitric acid or ice PSCs.

Before 12 June, the PSCs that formed

[1]NASA Ames Research Center, MS 245-4, Moffett Field, CA 94035–1000, USA. [2]NASA Jet Propulsion Laboratory, MS 183-701, Pasadena, CA 91109, USA. [3]Atmospheric and Environmental Research, Inc., 840 Memorial Drive, Cambridge, MA 02139–3794, USA. [4]Department of Meteorology, University of Edinburgh, Mayfield Road, Edinburgh, EH9 3JZ Scotland. [5]NASA Goddard Space Flight Center, Code 916, Greenbelt, MD 20904, USA. [6]Department of Physics, San Jose State University, One Washington Square, San Jose, CA 95192, USA. [7]Lockheed Martin Advanced Technology Center, 3251 Hanover Street, Palo Alto, CA 94304, USA.

*To whom correspondence should be addressed. E-mail: atabazadeh@mail.arc.nasa.gov

within the cold temperature contours, based on their thermal histories and vapor pressure behavior (*40*), were predominantly composed of supercooled ternary solution (STS) droplets of sulfuric acid, nitric acid, and water (Fig. 2). Because STS particles form by condensational growth, their average size remains below 0.5 μm in radius (*43*), making them inefficient in denitrifying the stratosphere. The existence of large micrometer-sized solid particles that initiate denitrification became evident in the CLAES aerosol

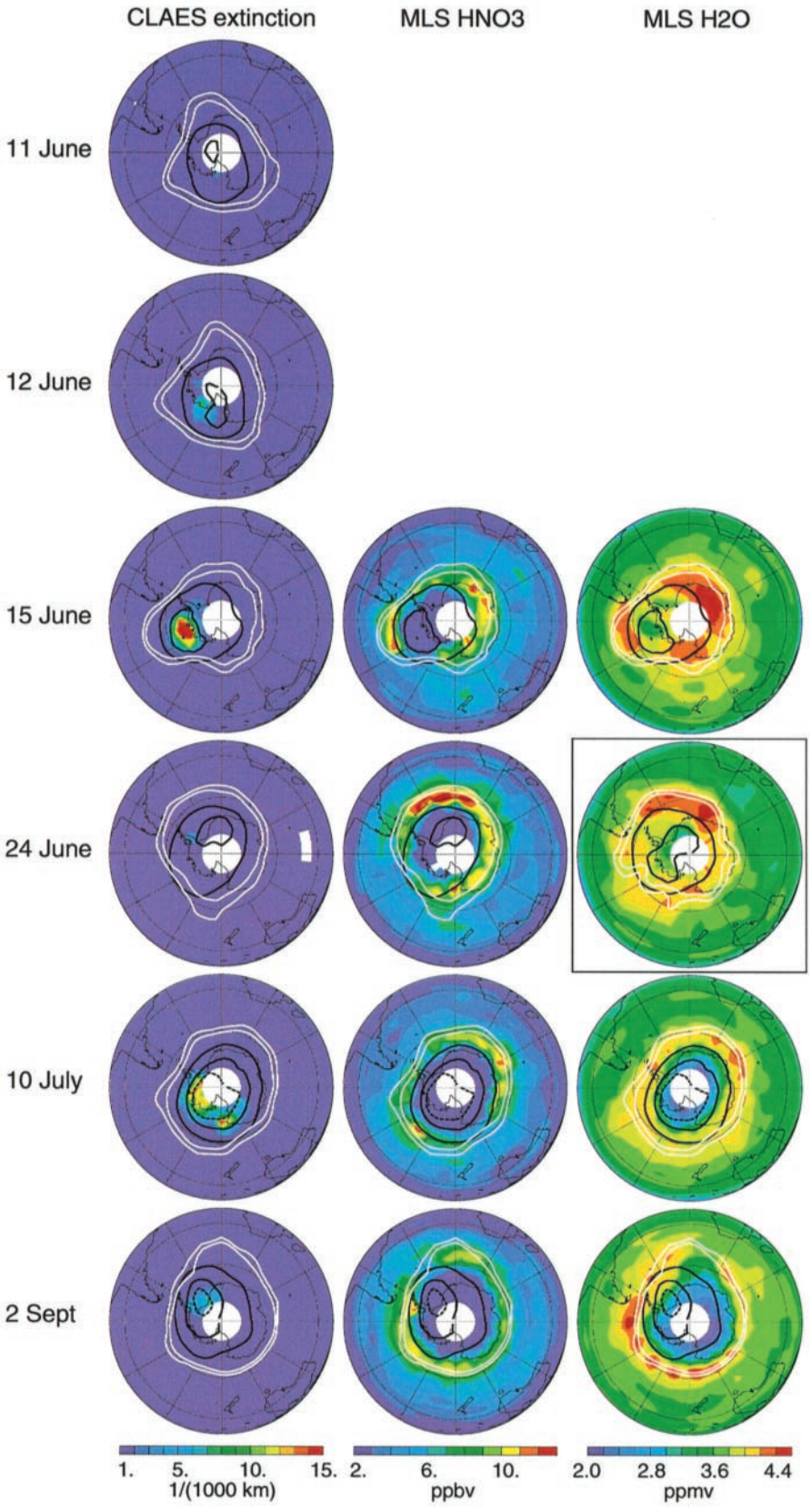

Fig. 1. Maps of CLAES aerosol extinction (at 12.82 μm) and MLS nitric acid and water vapor data for selected days during the 1992 Antarctic winter, interpolated onto the 450 K potential temperature surface using United Kingdom Meteorological Organization (UKMO) temperatures. The Antarctic winter of 1992 was used in this study because neither the CLAES instrument nor the MLS radiometer used to make stratospheric water vapor measurements were operational during the other southern winters. The thick black contours show UKMO temperatures at 195 and 188 K (the dashed black contour is at 185 K). Also superimposed (in white) on each of the maps are two contours of potential vorticity, calculated from UKMO temperature and geopotential height fields to show the boundaries of the vortex. The data versions used in this figure are V8, V4, and prototype V104 for CLAES, MLS nitric acid, and MLS water vapor, respectively. Problems with the UARS solar array caused a low-power situation that resulted in the MLS and CLAES instruments being turned off during the first part of June. CLAES began taking data again on 11 June, MLS on 15 June. However, to reduce power consumption the MLS water vapor instrument was switched off again on 20 June and remained off until 10 July, at which time operations returned to normal. The days for which the data are missing due to technical problems are left blank except for the 24 June water vapor map. The boxed map shown for this day is for 19 June, the last day in June that MLS measured water vapor. We have chosen the CLAES aerosol extinction scale to highlight the regions where solid PSCs are present above the levels expected for the growth of STS droplets (shown in purple) during this post-volcanic year.

extinction data on 12 June, so the onset of the denitrification process must have occurred after this day. By 15 June, the vapor pressure of nitric acid measured by MLS was more consistent with the presence of solid PSCs than STS droplets (*40*), indicating that by this day most of the nitric acid-containing cloud particles had been converted into solids.

The evidence for denitrification in Fig. 1 on 24 June is strong because temperature fields and the magnitude of nitric acid depletion, within the cold temperature contours, are similar on 15 June and 24 June. Yet the aerosol extinction is vastly different. The most likely explanation for the difference in the CLAES aerosol extinction data is that substantial amounts of nitric acid were removed irreversibly from the 450 K level between those dates, making it difficult for crystalline PSCs to form. For comparison, in Fig. 2 the change over time in gas phase nitric acid is shown for the 1992 Antarctic and the two coldest Arctic winters of the last decade (*22*). The Antarctic denitrification that occurs in late June persists throughout the late winter and early spring. In contrast, the lack of a noticeable change in gas phase nitric acid between early and late winter in the Arctic implies that denitrification as extensive as that in the Antarctic did not occur.

PSC lifetime statistics for four selected periods (marked in Fig. 2), including two Arctic winters, are shown in Fig. 3. The periods chosen for the Arctic analysis present the longest possible cloud lifetimes for the two coldest winters of the last decade during a consecutive 10-day period. The average crystalline PSC lifetimes for the Arctic and the early June Antarctic periods are similar (Fig. 3), and widespread denitrification is not apparent in the data for these study periods (Fig. 2). Because NAT (NAD) PSC lifetimes during Antarctic early June and the two Arctic winter study periods are about 6 to 8 (3 to 5) days, we suggest that a nucleation and growth time of at least 7 (4) days is required to selectively crystallize a ternary cloud into a few larger NAT (NAD) particles. Current PSC lifetimes are short in the Arctic because the areas of low temperature are usually confined to relatively small regions that are not concentric with the vortex, so air masses are rarely exposed to cold temperatures for extended periods. Doubling PSC lifetimes in the Arctic brings the exposure times to present Antarctic values during mid to late June when denitrification occurs (Fig. 3).

Denitrification at 450 K occurred in about 12 days (from 12 June to 24 June). Roughly 7 (4) days are required for effective crystallization and growth of a NAT (NAD) cloud. Thus, the actual sedimentation of the particles to lower levels must have occurred in about 5 (for a NAT cloud) to 8 (for a NAD cloud) days. The extinction on 24 June was low (similar to that shown in Fig. 1) at 68 mbar (2 to 3 km below the 450 K level) but not at 100 mbar (5 to 6 km below the 450 K level). At 100 mbar the extinction was about twice that expected from the hygroscopic growth of STS droplets at this level. Assuming a diabatic descent rate in the vortex of about 100 m per day (*44*), which would lead to 1.2-km large-scale descent in 12 days, the particles in the column must have sedimented at least 4 km in about 5 to 8 days for the 68 mbar level to show low extinction values on 24 June. The particle size needed for a sedimentation rate that leaves behind some particles at 100 mbar but not too many at 68-mbar is between 4 μm (NAD assumption) and 6 μm (NAT assumption) in radius. Selective growth of background aerosols to 4 to 6 μm is possible if solid particle number concentrations were about 0.005 to 0.01 cm^{-3}, in good agreement with the number concentrations measured by many balloons flown from McMurdo Station in the Antarctic (*45*, *46*).

Denitrification can be included in large-scale models by setting a NAT (NAD) nucleation time switch of ~7 (4) days [meaning that NAT (NAD) particles are produced in the model after an exposure time of ~7 (4) days below the NAT (NAD) point]. The NAT (NAD) particles produced after 7 (4) days can then sediment in the model at a rate of about 0.8 km (0.5 km) per day.

Another important point to address is whether ice is involved in the selective nucleation of large particles that result in denitrification. Statistics of many trajectories studied during the 12 June to 24 June period (Fig. 3) indicate that only a small fraction (<2 %) may have encountered ice nucleation temperatures [typically 3 K below the frost point (*37*, *47*, *48*)]. Thus, if ice formation were a requirement, then only a small fraction of the parcels would have experienced denitrification, contrary to the observations showing widespread denitrification on 24 June (Fig. 1). In addition, water vapor maps on 15 and 19 June (boxed map in Fig. 1) still do not indicate substantial water vapor depletion over vast areas, although some depletion is evident in small regions coincident with the coldest temperatures. Also the areas of water vapor depletion for the days shown are, in general, much smaller than the area of depleted nitric acid. All this evidence taken together strongly suggests that during this winter denitrification occurred without significant dehydration.

During the 1992 southern winter, the onset of severe dehydration at 450 K may have occurred after 27 June, when minimum temperatures dropped below the ice nucleation point over large areas (Fig. 2). By 10 July, the aerosol extinction on one side of the vortex corresponds well with the area of depleted water vapor mixing ratio, indicating the presence of Type II PSCs (ice clouds). The lack of correlation between aerosol extinction and low water vapor mixing ratios on the opposite side indicates that the air mass over this region was substantially dehydrated. This dehydration perhaps occurred over the region where the correlation still exists on 10 July because this air mass trajectory can be traced back to a location near the Palmer Peninsula (just to the west of the south pole) on or about 5 July. After 2 September, the aerosol extinction completely disappeared at this level. Our conclusion that substantial dehydration in the Antarctic begins in late June is supported by Antarctic balloon observations (*38*).

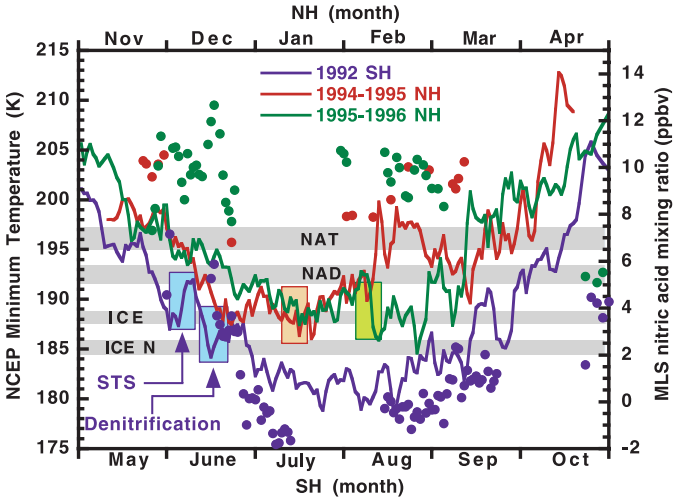

Fig. 2. Minimum National Centers for Environmental Prediction (NCEP) temperatures for selected winters at the 50-mbar pressure level, which is near the 450 K potential temperature surface. The periods for STS formation and denitrification during the Antarctic winter of 1992 are marked in the figure as blue boxes. The NAT, NAD, and ICE envelopes (shaded gray) show temperatures at which nitric acid and water saturate to form NAT, NAD and water ice particles, respectively. The ICE nucleation envelope marks the temperature at which ice clouds can nucleate in the stratosphere (*37*, *47*, *48*). The critical temperature envelopes are calculated for nitric acid and water vapor mixing ratios of 9 to 12 ppb and 4 to 5 ppm, respectively, based on in situ observations (*32*–*36*). Two Arctic study periods are also marked in the plot as orange and green boxes for the 1994–1995 and 1995–1996 winters, respectively. Symbols shown are time series of MLS gas phase nitric acid binned and averaged in the 75° to 80°S and 75° to 80°N bands for the Antarctic and the two Arctic winters, respectively.

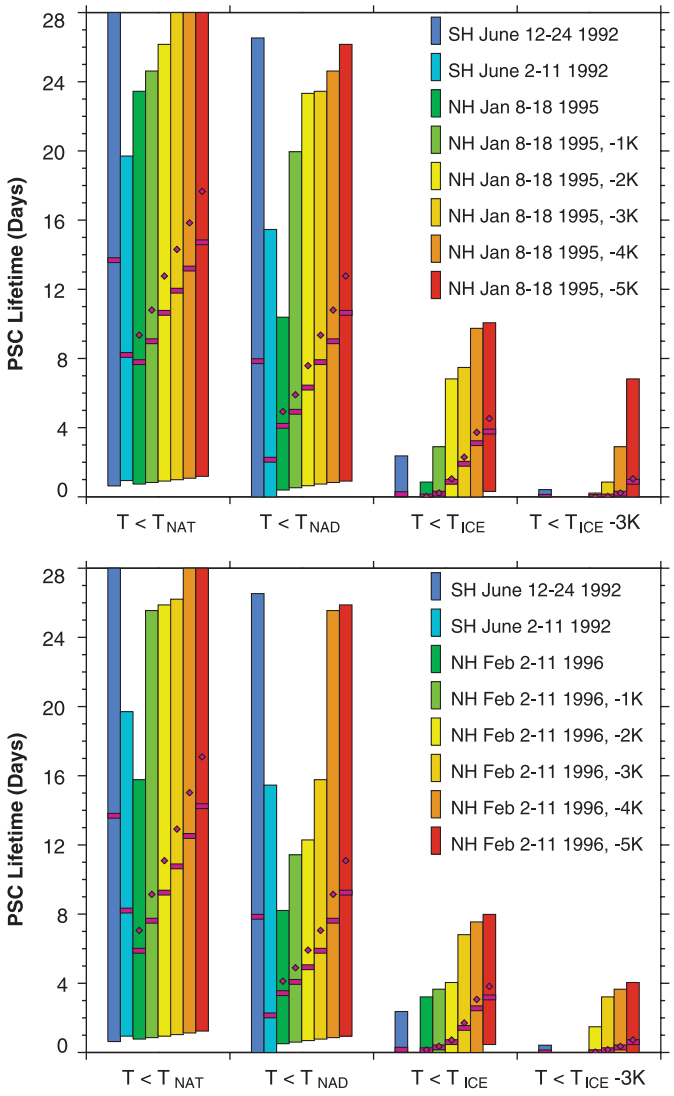

Fig. 3. Temperature statistics of over 3000 air mass trajectories for the study periods boxed in Fig. 2 at the 450 K potential temperature surface. To obtain cloud lifetimes for each temperature block 40 points were homogeneously distributed within the 192 K NCEP temperature contour for each day of the study period. The trajectories were then run forward and backward for each point to calculate how long temperatures stayed below the required values. For example, a total of 1040 trajectories were run for the 12 to 24 June Antarctic study period. The average cloud lifetime for each temperature block is shown as a horizontal magenta bar, which is constrained between the minimum and maximum lifetimes obtained for that entire study period. Also shown are Arctic cloud lifetime statistics for colder trajectories, which are colder than the original ones by increments marked on the plot. The mixing ratios used for the Antarctic calculations are 9 ppb for nitric acid and 4 ppm for water vapor. The mixing ratios used for the Arctic calculations are 12 ppb for nitric acid and 5 ppm for water vapor. The atmospheric concentrations used for the calculations are based on in situ observations (*32*–*36*). The diamonds show Arctic cloud lifetimes for an atmosphere containing 1 ppm more water vapor (6 ppm instead of 5 ppm).

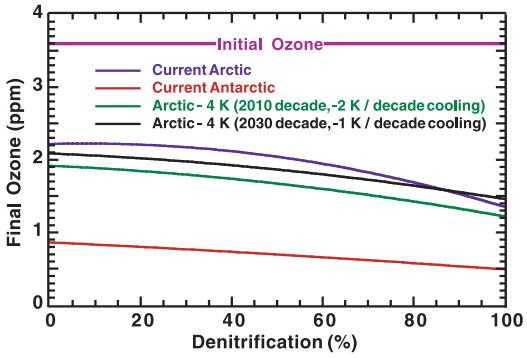

Fig. 4. Atmospheric and Environmental Research box model calculations of the springtime ozone mixing ratios (on 1 April and 1 November at 70°N and 70°S, respectively) as a function of denitrification in the air parcel. Initial ozone was set to 3.6 ppm as indicated. The typical 120-day-long Arctic and Antarctic trajectories used in the calculations are described in (*56*) and (*57*). The NAT PSC scheme is used in the calculations. Denitrification due to gravitational sedimentation of the nitric acid–containing particles occurs only during the PSC events (i.e., when $T < T_{NAT}$). For the same temperature history the intensity of denitrification is modulated in the model by producing different size particles during the PSC events for nitric acid removal out of the box. For the lines labeled "Arctic - 4 K", the temperature along the Arctic trajectory used is reduced by 4 K. Constant chlorine loading of 3 ppbv is used for the current and 2010 decade calculations. For the 2030 decade calculations the chlorine loading is reduced to 2.5 ppbv (*2*). A constant bromine loading of 20 parts per trillion by volume is used for all calculations (*2*, *56*).

In the future, the stratosphere may cool further due to changes in concentrations of greenhouse gases (*49*–*55*) such as carbon dioxide, water vapor, and ozone. Therefore, denitrification could occur in the Arctic as a result of both the cooling trends associated with greenhouse gases (*49*–*51*) and the increase in water vapor concentration (*52*, *53*) that directly enhances cloud formation. Because the exact cause of water vapor increase in the lower stratosphere is not known (*54*, *55*), it is difficult to speculate whether this trend will be sustained in the next few decades when temperatures are cold enough to promote denitrification in the Arctic. Here we performed sensitivity calculations for idealized air parcels (*25*, *56*, *57*) with and without enhanced levels of water vapor to define what future temperature and relative humidity fields may cause widespread Arctic denitrification.

Figure 3 illustrates that roughly a 4 to 5 K (3 to 4 K) decrease in temperatures experienced during the 1994–1995 and 1995–1996 Arctic winters would bring NAT (NAD) "PSC lifetimes" to present Antarctic values during mid to late June when denitrification occurs. Assuming water vapor mixing ratios are higher by 1 part per million (ppm), the magnitude of cooling needed for denitrification is reduced by roughly 1 K. Thus, the effect of 1 K cooling in promoting denitrification is equivalent to the effect of increasing the water vapor mixing ratio by 1 ppm. Overall for a lower stratospheric cooling rate of about 2 (1) K per decade (*49*–*51*), widespread severe denitrification may start to occur during the coldest winters of the 2010 (2030) decade.

A photochemical box model (*56*, *57*) with a complete heterogeneous chemistry package was used to investigate the sensitivity of Arctic ozone loss to denitrification. To validate the model, we first calculated the magnitude of ozone loss attributed to denitrification for typical Antarctic and Arctic air parcels (Fig. 4). The magnitude of ozone loss calculated for current conditions, with and without denitrification, is in good agreement with the results from large-scale model simulations (*58*–*60*) and other box model studies (*25*). Figure 4 shows that denitrification in excess of 50% is required for the process to start having an impact on Arctic ozone. Because the Arctic stratosphere has not yet been cold enough for extensive denitrification to occur, we performed sensitivity calculations for future Arctic winters that are colder than the current ones by 4 K. In the absence of denitrification, the calculated ozone loss is about 1.7 ppm (green line) and 1.5 ppm (black line), whereas for complete denitrification the ozone is further reduced by about 0.7 ppm (green line) and 0.6 ppm (black line) for the 2010 and 2030 decades, respectively. Because complete denitrification is unlikely even in the Antarctic (*22*), the enhancement in Arctic

ozone loss due to denitrification is limited to below ~30% [i.e., 0.7 ppmv additional loss divided by (1.7 + 0.7) ppmv total loss for the 2010 decade].

The prospect of widespread Arctic denitrification in the future is real even if lower stratospheric temperatures are cooling at a rate of only 1 K per decade. The development of a persistently cold and stable vortex is not required for Arctic denitrification to occur. For Arctic denitrification to be initiated, longer PSC lifetimes, similar to those of the Antarctic during mid to late June, need to be maintained only for periods less than 2 weeks. Widespread severe denitrification could enhance future Arctic ozone loss by up to 30%. Overall, though, the role of denitrification in the depletion of Arctic ozone in large-scale models is still uncertain, and the effect of changes in temperature and water vapor on denitrification needs to be quantified to better understand and predict Arctic ozone trends.

References and Notes

1. S. Solomon, *Rev. Geophys.* **37**, 275 (1999).
2. *WMO Scientific Assessment of Ozone Depletion: 1998, Rep. 44* (1999).
3. O. B. Toon, P. Hamill, R. P. Turco, J. Pinto, *Geophys. Res. Lett.* **13,** 1284 (1986).
4. P. J. Crutzen and F. Arnold, *Nature* **324**, 651 (1986).
5. R. J. Salawitch, G. P. Gobbi, S. C. Wofsy, M. B. McElroy, *Nature* **339**, 525 (1989).
6. R. S. Stolarski, *Nature* **389**, 788 (1997).
7. W. H. Brune *et al.*, *Science* **252**, 1260 (1991).
8. W. H. Brune, D. W. Toohey, J. G. Anderson, K. R. Chan, *Geophys. Res. Lett.* **17**, 505 (1990).
9. C. R. Webster *et al.*, *Science* **261**, 1130 (1993).
10. D. W. Toohey *et al.*, *Science* **261**, 1134 (1993).
11. M. L. Santee *et al.*, *Science* **267**, 849 (1995).
12. J. W. Waters *et al.*, *Nature* **362**, 597 (1993).
13. D. G. Andrews, *Pure Appl. Geophys.* **130**, 213 (1989).
14. D. W. Waugh and W. J. Randel, *J. Atmos. Sci.* **56**, 1594 (1999).
15. M. Rex *et al.*, *Nature* **389**, 835 (1997).
16. N. Larsen *et al.*, *Geophys. Res. Lett.* **21**, 1611 (1994).
17. G. L. Manney *et al.*, *Nature* **370**, 429 (1994).
18. G. L. Manney, *Geophys. Res. Lett.* **23**, 85 (1996).
19. _____ *et al.*, *Geophys. Res. Lett.* **24**, 2697 (1997).
20. G. L. Manney *et al.*, *J. Atmos. Sci.* **52**, 3069 (1995).
21. M. P. Chipperfield and R. L. Jones, *Nature* **400**, 551 (1999).
22. M. L. Santee, G. L. Manney, L. Froidevaux, W. G. Read, J. Waters, *J. Geophys. Res.* **104**, 8225 (1999).
23. A. E. Dessler, J. Wu, M. L. Santee, M. R. Schoeberl, *J. Geophys. Res.* **104**, 13993 (1999).
24. A. E. Roche *et al.*, *J. Atmos. Sci.* **51**, 2877 (1994).
25. A. E. Waibel *et al.*, *Science* **283**, 2064 (1999).
26. D. W. Waugh, *J. Geophys. Res.* **102**, 13119 (1997).
27. H. A. Michelsen, G. L. Manney, M. R. Gunson, R. Zander, *J. Geophys. Res.* **103**, 28347 (1998).
28. Y. Kondo *et al.*, *J. Geophys. Res.* **104**, 8215 (1999).
29. G. L. Manney *et al.*, *J. Geophys. Res.* **104**, 18841 (1999).
30. M. Rex *et al.*, *J. Geophys. Res.* **104**, 26611 (1999).
31. R. A. Plumb, D. W. Waugh, M. P. Chipperfield, *J. Geophys. Res.* **105**, 10062 (2000).
32. D. W. Fahey *et al.*, *Nature* **344**, 321 (1990).
33. S. R. Kawa *et al.*, *J. Geophys. Res.* **97**, 7925 (1992).
34. H. Fischer *et al.*, *J. Geophys. Res.* **102**, 23559 (1997).
35. H. F. Schlager and F. Arnold, *Geophys. Res. Lett.* **17**, 433 (1990).
36. F. Arnold, V. Buger, K. Gollinger, M. Roncossek, *J. Atmos. Chem.* **30**, 49 (1998).
37. K. S. Carslaw *et al.*, *J. Geophys. Res.* **103**, 5785 (1998).
38. H. Vomel, S. J. Oltmans, D. J. Hofmann, T. Deshler, J. M. Rosen, *J. Geophys. Res.* **100**, 13919 (1995).
39. K. S. Carslaw *et al.*, *Nature* **391**, 675 (1998).
40. M. L. Santee *et al.*, *J. Geophys. Res.* **103**, 13285 (1998).
41. H. C. Pumphrey, *J. Geophys. Res.* **104**, 9399 (1999).
42. J. L. Mergenthaler, J. B. Kumer, A. E. Roche, S. T. Massie, *J. Geophys. Res.* **102**, 19161 (1997)
43. A. Tabazadeh, R. P. Turco, K. Drdla, M. Z. Jacobson, O. B. Toon, *Geophys. Res. Lett.* **21**, 1619 (1994).
44. M. R. Schoeberl *et al.*, *J. Geophys. Res.* **97**, 7859 (1992).
45. D. J. Hofmann and T. Deshler, *J. Geophys. Res.* **96**, 2897 (1991).
46. T. Deshler, A. Adriani, D. J. Hofmann, G. P. Gobbi, *Geophys. Res. Lett.* **18**, 1999 (1991).
47. H. A. Chang, T. Koop, L. T. Molina, M. J. Molina, *J. Phys. Chem.* **103**, 2673 (1999).
48. A. Tabazadeh, S. T. Martin, J. S. Lin, *Geophys. Res. Lett.* **27**, 1111 (2000).
49. S. Pawson and B. Naujokat, *Geophys. Res. Lett.* **24**, 575 (1997).
50. V. Ramaswamy, M. D. Schwartzkopf, W. Randel, *Nature* **382**, 616 (1996).
51. D. T. Shindell, D. Rind, P. Lonergan, *Nature* **392**, 589 (1998).
52. S. J. Oltmans and D. J. Hofmann, *Nature* **374**, 146, (1995).
53. G. E. Nedoluha *et al.*, *J. Geophys. Res.* **103**, 3531 (1998).
54. S. J. Evans, R. Toumi, J. E. Harries, M. P. Chipperfield, J. M. Russell III, *J. Geophys. Res.* **103**, 8715 (1998).
55. P. M. de F. Forster and K. P. Shine, *Geophys. Res. Lett.* **26**, 3309 (1999).
56. M. Y. Danilin, N. D. Sze, M. K. W. Ko, J. M. Rodrigiez, A. Tabazadeh, *Geophys. Res. Lett.* **25**, 2141 (1998).
57. M. Y. Danilin, N. D. Sze, M. K. W. Ko, J. M. Rodrigiez, M. J. Prather, *Geophys. Res. Lett.* **23**, 153 (1996).
58. G. P. Brasseur, X. Tie, P. J. Rasch, F. Lefevre, *J. Geophys. Res.* **102**, 8909 (1997).
59. R. W. Portmann *et al.*, *J. Geophys. Res.* **101**, 22991 (1996).
60. M. P. Chipperfield and J. A. Pyle, *J. Geophys. Res.* **103**, 28389 (1998).

61. We thank G. Manney, D. Kinnison, M. Tolbert, and K. Drdla for helpful comments and suggestions. Supported by NASA's Upper Atmosphere Research Satellite (UARS) program and a Presidential Early Career Award for Scientists and Engineers (A.T.). The work at the Jet Propulsion Laboratory was done under contract with NASA. M.Y.D. is supported by NASA Atmospheric Chemistry Modeling and Analysis Program (ACMAP) and UARS guest investigator programs. H.C.P. was supported by UK Natural Environment Research Council grant GR3/10111.

15 November 1999; accepted 12 April 2000

Field Measurement of Slow Metamorphic Reaction Rates at Temperatures of 500° to 600°C

Ethan F. Baxter* and Donald J. DePaolo

High-temperature metamorphic reaction rates were measured using strontium isotopic ratios of garnet and whole rock from a field site near Simplon Pass, Switzerland. For metamorphic conditions of cooling from 612° ± 17°C to 505° ± 15°C at pressures up to 9.1 kilobars, the inferred bulk fluid-rock exchange rate is $1.3^{+1.1}_{-0.4} \times 10^{-7}$ grams of solid reacted per gram of solid per year, several orders of magnitude lower than laboratory-based estimates. The inferred reaction rate suggests that mineral chemistry may lag the evolving conditions in Earth's crust during mountain building.

Chemical and isotopic compositions of metamorphic minerals are used to determine the history of pressure, temperature, and chemical (P-T-X) evolution in Earth's crust during mountain building. Data interpretation is based on the assumption of local equilibrium (*1*), which requires that reactions proceed rapidly relative to rates of local P-T-X change. Whether this assumption is warranted is difficult to ascertain. Extrapolation of existing laboratory-based kinetic data (*2*–*5*) to natural systems is subject to large uncertainties because the reaction mechanisms (*4*) and controlling parameters (e.g., departure from equilibrium and reactive surface area) are unknown. There is growing recognition of natural effects attributable to slower reaction rates (*6, 7*), but no direct determinations of regional metamorphic reaction rates have been made.

Here, Sr isotopic measurements in metamorphic rocks are used in conjunction with geochronology and numerical models to estimate natural rates of chemical exchange between minerals and intergranular fluid [more generally, the intergranular transporting medium or ITM (*8*)]. The approach focuses on analysis of isotopic variations along a transect normal to a lithologic contact where there was, before metamorphism, a sharp, step-like contrast in isotopic ratios. During metamorphism, the isotope ratio ($^{87}Sr/^{86}Sr$) profile across the contact changes in different ways depending on the relative rates of cross-contact intergranular transport and local solid-ITM exchange (*7*). Local chemical reactions are mediated by the ITM as solid dissolves and reprecipitates. The isotope ratio is a passive tracer of the bulk solid reactivity. The driving potential for the bulk solid reaction is

Department of Geology and Geophysics, University of California, 301 McCone Hall, Berkeley, CA 94720, USA.

*To whom correspondence should be addressed. E-mail: ebaxter@uclink4.berkeley.edu